

# A Bulky Imidodiphosphorimidate Brønsted Acid Enables Highly Enantioselective Prins-semipinacol Rearrangements

Junshan Lai and Jolene P. Reid\*

Department of Chemistry, University of British Columbia, Vancouver, British Columbia V6T 1Z1, Canada

**ABSTRACT:** The development of BINOL-derived Brønsted acid catalysts has been profoundly guided by rational design, with carefully implemented structural changes leading to unique generations of catalysts with enhanced reaction capabilities. This approach to catalyst optimization has promoted the integration of knowledge gathered in optimizing prior eras of Brønsted acids and ultimately, the molecular features that have contributed to the success of previous designs are preserved. Of these, the large substituents at the 3 and 3' positions of the BINOL backbone are the most critical with almost every newly developed structure possessing this feature. However, imidodiphosphorimidate (IDPi) catalysts are not synthetically well-suited to contain the same sterically bulky groups associated with the high selectivity imparted by previously implemented catalyst structures. Herein, we have leveraged the moderate size (as compared to TRIP and 9-anthryl) but high applicability of the 9-phenanthryl substituent to synthesize a sterically demanding IDPi. Using computed descriptors, we survey the catalyst properties of known structures to demonstrate this catalyst to be both unique and one of the bulkiest IDPi yet synthesized. The applicability of the catalyst was evaluated in the construction of stereochemically dense spirocycles generated via an asymmetric Prins-semipinacol reaction sequence. Transition state calculations were deployed to interrogate the origins of the superior enantioselectivity and these demonstrate the mechanistic hallmarks of the 9-phenanthryl substituent can be generalized to a genuinely different class of Brønsted acid catalyst. Ultimately, providing the basis for the development of general catalyst design principles and the translation of “privileged” substituents across unique eras of Brønsted acid catalysts structures.

## Introduction

The structure of chiral organocatalysts continues to evolve with each notable design gaining enhanced function over enantioselective bond construction.<sup>1–2</sup> Asymmetric Brønsted acid catalysis exemplifies this where iterative changes to the catalyst structure has enabled marked increases in selectivity and reactivity for a diverse set of organic transformations.<sup>3–5</sup> Indeed, these efforts have led to generations of rational catalyst designs that have developed from simple modifications of the catalyst substituents<sup>6</sup> to the introduction of strongly acidic dimeric catalyst structures (Figure 1).<sup>7–8</sup> Despite this significant progression in structure, new Brønsted acid catalysts typically retain the key molecular features that have led to a good performance with older designs. For example, N-triflyl phosphoramidate catalysts were introduced to overcome the reactivity barriers associated with weakly basic carbonyl substrates but contain the same sterically bulky groups associated with the high selectivity imparted by BINOL-derived phosphoric acids.<sup>9</sup> Likewise, List's imidodiphosphates (IDP) enable highly enantioselective transformations of difficult substrates through the strict conformational confinement generated by the two binaphthol units and constrained by the same large substituents at the 3 and 3' positions.

This leads to the questions: 1) Considering the commonality in catalyst substituent structure across distinct eras of Brønsted acid catalyst can similar reasons for stereocontrol be invoked? If so, 2) how can this information

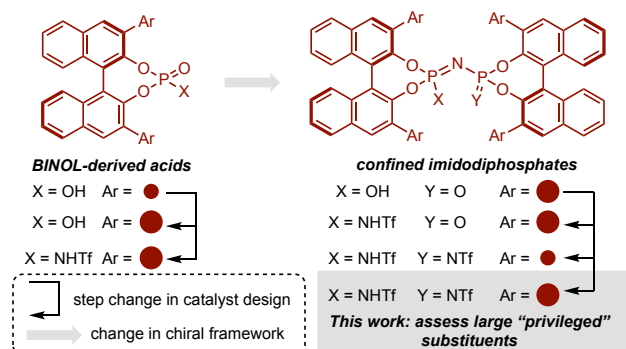


**Figure 1.** The evolution of Brønsted acid catalysts for enantioselective bond construction.

be leveraged for the development of selective catalyst structures? And 3) Do these catalysts bearing “privileged” substituents facilitate reactions that have not yet been rendered highly enantioselective? We confront these questions in this present study, and report the results of a highly acidic and strongly confined acid catalyst bearing 9-phenanthryl substituents for the enantioselective synthesis of spirocycles via a Prins-semipinacol rearrangement. DFT calculations reveal that the stereocontrolling features of the 9-phenanthryl substituent can be generalized to a different class of Brønsted acid catalyst.

The context for this study is in the area of imidodiphosphorimidate (IDPi) catalysts,<sup>10</sup> as this type of catalyst structure has not yet benefitted from the knowledge gathered in optimizing previous eras of Brønsted acids. In other words, the substituents at the 3,3' positions are usually distinctive showing little structural overlap with the previous generations of Brønsted acids. To our knowledge, the effect of including the large 3,3' groups typically associated with earlier catalyst designs has not been assessed, although this is largely because the chiral framework tends not to be synthetically well-suited to containing functionality that places additional steric bulk proximal to the phosphorous atom. The synthesis of these catalysts are challenging usually relying on a dimerization step which is strongly influenced by the steric properties of the 3,3'-substituents, if these are too big unsatisfactory yields are obtained or the reaction may fail to proceed altogether.<sup>11</sup> However, it might be possible to attach moderately sized substituents that have previously worked well with earlier catalyst designs and leverage the resulting IDPi for selective catalysis.

## Results and Discussion.

**Trends and Molecular Descriptors.** To implement this “privileged” substituent approach for prioritizing the catalysts to be synthesized, key evaluation criteria will need to be defined. In this context, the structure of the substituents at the 3,3' positions of the BINOL backbone have a considerable effect on the stereochemical outcome of many reactions, and, usually, large steric bulk is required for high enantioselectivity.<sup>12-14</sup> Of these the most general Brønsted acid structures possess either very large alkyl groups at the 2, 4 and 6 positions of the aromatic ring or contain extended  $\pi$ -systems (i.e. 9-anthryl or 9-phenanthryl). As such, catalysts bearing these “privileged” Brønsted acid substituents should be selected first for synthesis and screening. However, IDPi catalysts containing excessive steric demands at the 3,3' positions are not readily synthetically accessible. On this basis, we questioned what is the largest “privileged” Brønsted acid substituent that can be incorporated into the IDPi catalyst framework? To answer this question, we considered the size of 3,3' aromatic groups common to many Brønsted acids using two different measures of steric requirements (i) rotation barrier for a phenyl group, and (ii) A Remote Environment Angle: AREA( $\theta$ ), a measure of space less close to the catalyst site.<sup>12</sup> At this initial stage of the study we are only concerned about the steric features exhibited by a portion of the IDPi catalyst such that these values do not need to be obtained from the whole molecule structure. Indeed, rotational barriers for a phenyl group are derived from the energy required for rotation around the central C–C bond. Because the interaction between the R groups and the hydrogens on the opposing aryl ring are responsible for the destabilization of the eclipsed conformation this descriptor can only account for nearby sterics. In contrast, the angle measurement AREA( $\theta$ ), is sensitive to increases in the steric demands remote from the aromatic ring with substituents that crowd access to the phosphorus resulting in smaller values. To estimate if the incorporation of certain substituents could lead to a structure that would be both well performing and synthetically tractable, we next

considered how these groups fit and operate within existing catalyst space. Visual inspection of reported IDPi catalysts, shows that 3,3' substituents only display a large structural variation in the remote positions of the aromatic ring. Although IDPis bearing ethyl and methyl groups at the 2,4,6 positions of the 3,3'-aromatic ring are known, their catalytic performance has not yet been evaluated. Therefore, the impact of introducing steric demands at positions close to the phosphorous is less clear, however, it is expected to lead to highly reactive and selective catalysts based on the information gathered from structurally familiar catalyst types. Key data is summarized in Figure 2B. These results indicate that among the substituents that have worked with previous Brønsted acids the 9-phenanthryl is the only group that bears steric demands similar to known IDPi structures (i.e. those bearing 1-naphthyl and 2-naphthyl substituents).

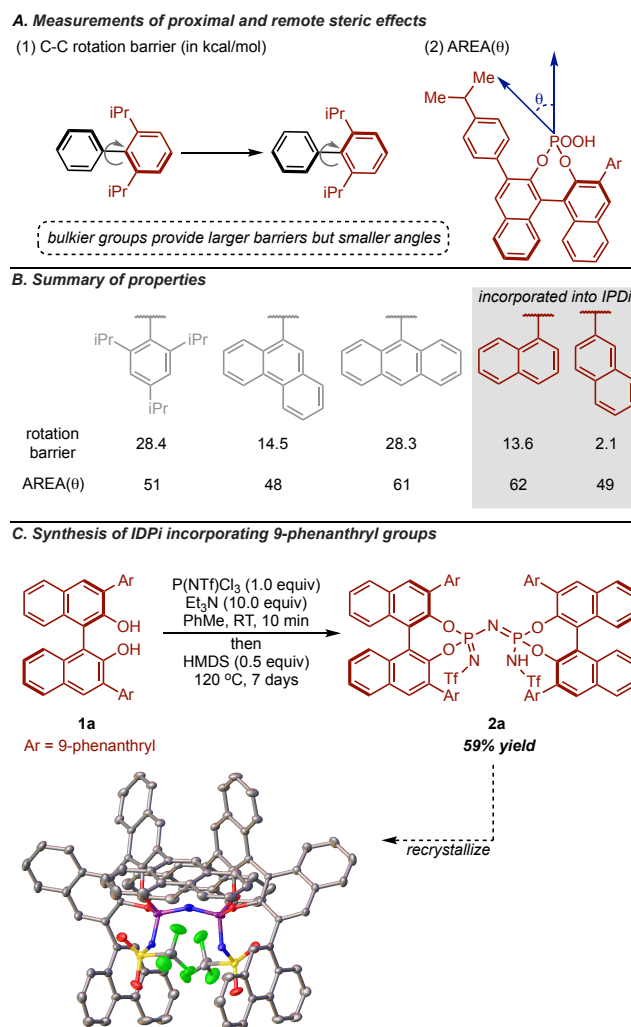


**Figure 2.** (A) Catalyst parameters evaluated in this study. Steric parameter (1) measures nearby bulk while (2) AREA( $\theta$ ), accounts for steric effects distant from the phosphoric acid moiety. (B) Determining the synthetic feasibility of larger and more general catalyst groups. Note IDPis bearing the substituents in the grey box have been previously synthesized. (C) Synthesis and structural analysis of an IDPi catalyst structure containing large 9-phenanthryl groups.

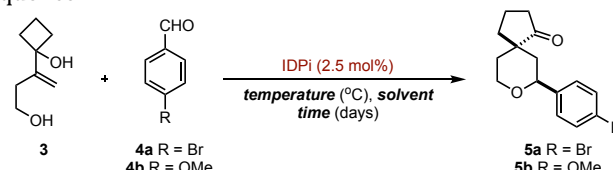
For example, the structural descriptors show that the proximal steric effect exerted by 9-phenanthryl will be similar to that of the 1-naphthyl substituent while the remote steric bulk is measured to be comparable to the 2-naphthyl group. This may be surprising and it is possible that the perceived significantly larger size of a 9-phenanthryl substituent has inhibited the investigation of these catalysts thus far. Intriguingly, this comparison also suggests that installing a 9-phenanthryl substituent upon the IDPi framework could allow access to one of the bulkiest catalyst structure yet prepared (i.e. most catalysts contain hydrogen atoms at the 2 and 6 positions of the 3,3'-aromatic ring, see SI).

Motivated by the structural uniqueness afforded by this catalyst we attempted to synthesize the novel IDPi bearing a 9-phenanthryl group. The List group has reported several ways that enable access to this catalyst motif with the most common approach involving dimerization of the 3,3'-substituted BINOL-derivatives in the presence of an ammonia surrogate.<sup>15-17</sup> This factor, combined with the observation that particular IDPis containing substituents with similar steric features can be accessed in this manner, prompted us to explore the reactivity of the requisite 3,3'-substituted BINOL-derivative. Using this procedure we synthesized IDPi **2a**, obtaining 59% yield after 7 days (Figure 2C). This result is comparable to the synthesis of other IDPis which typically require prolonged reaction times of 3–4 days.<sup>18-19</sup> Attempted improvements to the catalyst synthesis focused on employing a recent strategy developed by the List group which have shown impressive outcomes in accessing sterically hindered catalysts.<sup>11</sup> Unfortunately, our efforts in applying this method to the synthesis of **2a** did not yield desirable results. Structural crystallographic analyses of the imidodiphosphorimidate **2a** reveals a highly confined chiral pocket created by the two BINOL backbones and constrained by the large 3 and 3' substituents (Figure 2C).

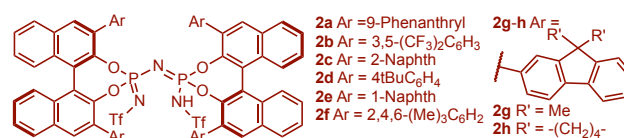
**Catalytic application.** Having produced a Brønsted acid confined within a sterically demanding chiral cavity, we examined the catalyst's aptitude to enforce high levels of enantiofacial discrimination for a continuous series of selective reactions. Because a single chiral catalyst must enable stereocontrol over discrete reaction events this approach to chiral molecule construction is much less common and to our knowledge, no examples have been reported with IDPis. These factors make sequential reactions an appealing assessment of the catalyst's ability to facilitate a difficult chemical transformation. In this context, we identified a Prins-semipinacol rearrangement as a stringent test that involves structurally unique reactive intermediates and bond forming steps to produce stereochemically dense spirocycles. In accord with previous studies,<sup>20-22</sup> we surmised that upon exposure of an aldehyde with a homoallylic alcohol an acid-catalyzed cyclocondensation would generate a carbocation and trigger a stereoselective skeletal rearrangement through the migration of the  $\sigma$ -bond. Central to the utility of this reaction sequence is the mechanistic requirement that

any selectivity imparted in the semipinacol step is reinforced not eroded by the catalyst structure. Specifically, this would ensure high levels of diastereoselectivity for the overall process regardless of the stereochemistry set in the first key catalytic step. With this mechanistic print in mind, our investigation began by subjecting homoallylic alcohol **3** with aldehyde **4a** to the reaction conditions shown in Table 1. A catalyst evaluation showed popular IDPi's to provide insufficient enantioselectivities while our sterically bulky IDPi provided encouraging results (Table 1 entries 1-4 and 11). In more detail, catalyst structures **2b-2h** have all proved to be valuable in generating a diverse range of chiral compounds with high-levels of stereoselectivity. Ultimately, each catalyst has been confirmed to be optimal for at least one reaction type rendering these structures as important benchmarks for evaluating **2a** in this reaction.

**Table 1.** Optimization of the Prins-semipinacol reaction sequence.<sup>a</sup>

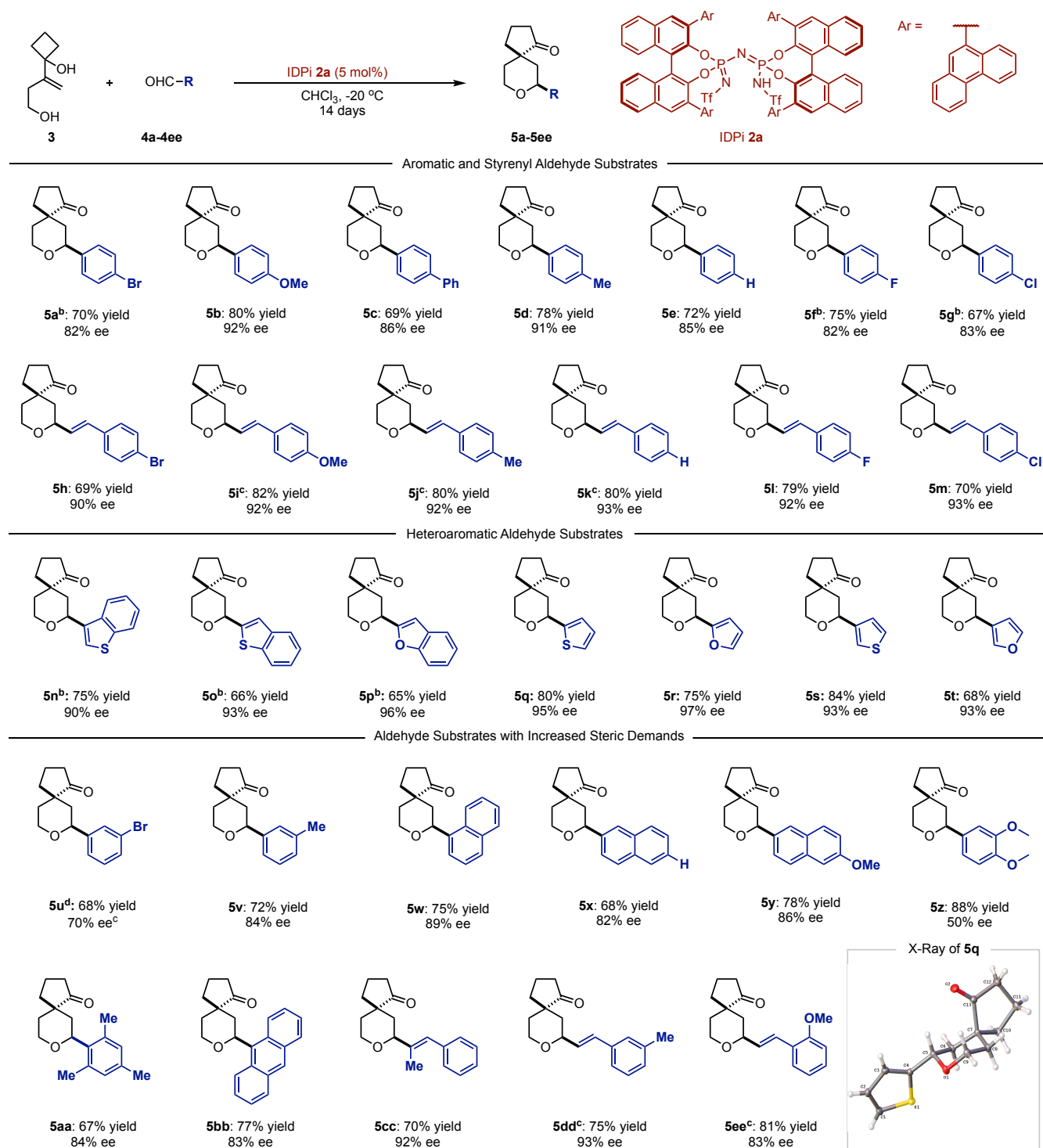


entry	R	IDPi	Temperature	Solvent	Time	Yield (%)	ee <sup>d</sup> (%)
1	Br	2a	RT	DCM	3	80	60
2	Br	2b	RT	DCM	3	79	30
3	Br	2c	RT	DCM	3	85	32
4	Br	2d	RT	DCM	3	82	14
5	Br	2e	RT	DCM	3	70	0
6	Br	2f	RT	DCM	6	20	5
7	Br	2g	RT	DCM	3	78	45
8	Br	2h	RT	DCM	3	83	53
9	Br	2a	RT	PhMe	3	72	66
10	Br	2a	RT	PhH	3	72	68
11	Br	2a	RT	DCE	3	80	46
12	Br	2a	RT	Et <sub>2</sub> O	3	80	32
13	Br	2a	RT	CHCl <sub>3</sub>	3	86	76
14 <sup>e</sup>	Br	2a	0	CHCl <sub>3</sub>	14	70	82
15	OMe	2a	0	CHCl <sub>3</sub>	7	85	86
16 <sup>e</sup>	OMe	2a	-20	CHCl <sub>3</sub>	14	80	92



<sup>a</sup>Reactions were run with the following conditions: **3** (14.2 mg, 0.1 mmol, 1.0 eq), the aldehyde **4a** or **4b** (0.12 mmol, 1.2 eq) IDPi (2.5 mol%), solvent (0.5 mL). All reactions proceed with >99:1 dr. <sup>b</sup>Isolated yields given. <sup>c</sup>Enantioselectivities (ee) were measured by SFC. <sup>d</sup>Reactions run with 5 mol% catalyst loading. See the Supporting Information for further details.

**Scheme 1.** Various aldehyde substrates tested with the optimal conditions.<sup>a</sup>

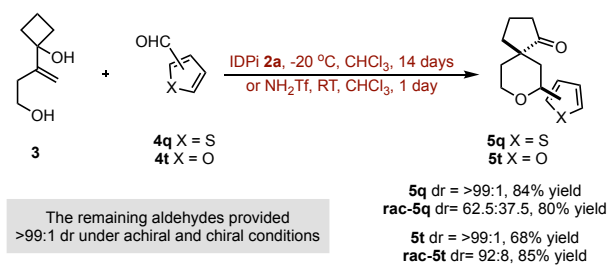


<sup>a</sup> Reaction conditions: **3** (14.2 mg, 0.1 mmol, 1.0 eq), the aldehyde **4a-4ee** (0.12 mmol, 1.2 eq) IDPi (5 mol%),  $\text{CHCl}_3$  (0.5 mL). All reactions proceed with >99:1 dr. Isolated yields given. Enantioselectivities (ee) were measured by SFC. Absolute configurations confirmed by the X-ray crystallographic analysis after recrystallization of **5q**. The stereochemistry of the remainder of the entries is assigned by analogy.<sup>b</sup> Reactions were conducted at  $0^\circ\text{C}$  for 14 days.<sup>c</sup> Reactions were conducted at  $-20^\circ\text{C}$  for 12 days.<sup>d</sup> Reactions were conducted at rt for 7 days.

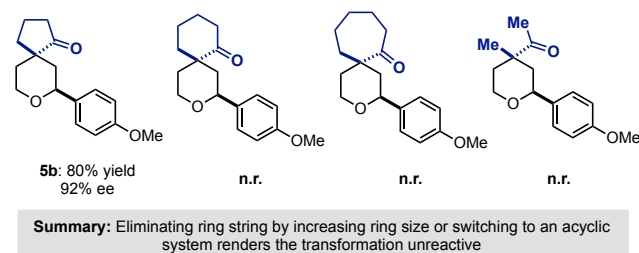
While extended commentary could be provided about each individual result, significant conclusions pointed to the critical nature of having a large catalyst substituent that can also engage in attractive noncovalent interactions. This is further confirmed by the poor result obtained with the sterically bulky catalyst **2f** (rotation barrier 21.6 kcal/mol, AREA(0) of 61°). Further, these observations with IDPis are consistent with our previous studies focused on understanding chiral phosphoric acids trends. These demonstrated catalysts that bear large alkyl groups at the 2, 4 and 6 positions of the aromatic ring primarily control the product outcome through steric contacts. While catalysts containing extended  $\pi$ -systems like 9-phenanthryl do not rely on a single set of noncovalent interactions to impart enantioinduction. In other words, because these catalysts bear large groups with polarizable surfaces, they can facilitate high levels of enantioselectivity by engaging in both attractive and repulsive noncovalent contacts. These results could imply that this is a key mechanistic feature of the group rather than a particular catalyst structure. In returning to the optimization, we discovered that switching the solvent to  $\text{CHCl}_3$  and lowering the temperature allowed the spirocycle to obtain in 82% ee (Table 1 entry 10). Motivated by these results, further improvements to the enantioselectivity was achieved by decreasing the temperature from 0 °C to -20 °C but this tactic was limited to more reactive, electron rich aldehydes (Table 1 entry 13). Having developed optimal conditions for this new enantioselective Prins-semipinacol rearrangement sequence, we next examined the scope of the aldehyde component. As shown in Scheme 1, variations of the aryl component were generally well tolerated, although products bearing strongly electron withdrawing substituents were generated with lower enantioselectivities due to the higher temperature requirement. This lower reactivity with electron poor substrates is notable and consistent with a cationic charge developing in the rate determining step.

## Scheme 2. Miscellaneous experiments

### A. Impact of the catalyst on the selectivity of the reaction



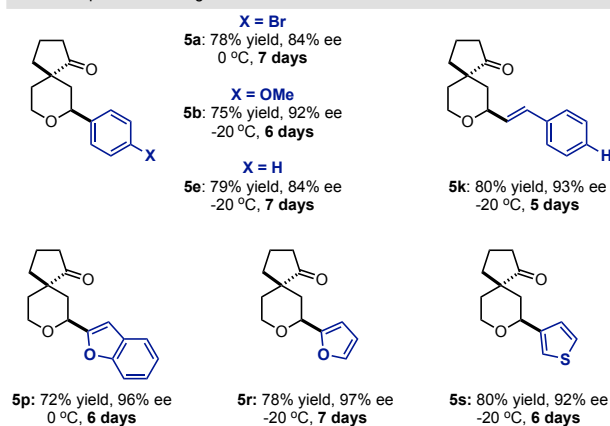
### B. Effect of ring strain



Indeed, substrates with even greater electron withdrawing capabilities (e.g. CN and  $\text{NO}_2$ ) failed to react at room temperature. A similar lack of reactivity was discovered when assessing various aliphatic substrates (see SI for more details). Exploration of styrenyl aldehydes showed less sensitivity to the electronic features of the aromatic ring having produced high levels of enantioselectivity across a diverse set of substrates. To round out this aldehyde survey, we examined the use of heteroaromatics in the reaction relay. When progressing to this substrate class, we obtained some of the highest enantioselectivities observed thus far in any IDPi catalyzed reaction. Aldehydes bearing sterically demanding substituents also proved less selective and this may reflect the inability of our strictly confined acid to efficiently accommodate large substrates. The exquisite selectivity imparted by our confined catalyst is highlighted on comparing the diastereoselectivity created in the semipinacol rearrangement under achiral and chiral conditions. More specifically, the data presented in Scheme 2 shows that the catalyst control matches the inherent stereoselectivity preference and were possible, enriches the selectivity. Further reaction insight was obtained from evaluating several designed homoallylic alcohols. The failure of these systems to react supports the crucial role of ring strain relief in driving the reaction forward. To focus our efforts on shortening the long reaction times we evaluated increasing the catalyst loadings with a small set of representative structures. Doubling the amount of catalyst employed dramatically shortened the reaction times and afforded products in comparable yields and enantioselectivities (Scheme 3). Importantly, the catalyst could be recovered from these processes and reused without loss of efficiency.

## Scheme 3. Shortening reaction times with increased catalyst loading.<sup>a</sup>

### Prins-semipinacol rearrangement with 10 mol% IDPi **2a**



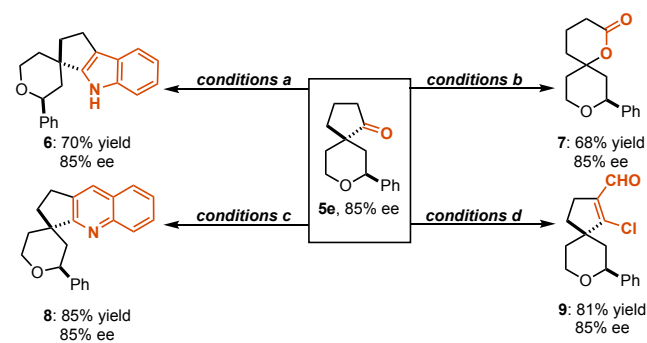
<sup>a</sup> Reactions were run with IDPi (10 mol%) under otherwise identical conditions to those shown in Scheme 2.

One limitation to acknowledge is that variations to the allylic alcohol **3** are not possible as highlighted by the results in Scheme 2B. Accordingly, we sought to expand the utility of the products in a set of synthetic elaborations (Scheme 4). Visual analysis of the X-ray structure of **5q** shows the distinctive feature that both prochiral faces of the ketone are



relatively unhindered. This suggests that the spirocycles would react with little substrate diastereocontrol. As such our diversification studies focused on molecular changes that did not introduce a third stereocenter. As a first assessment we questioned if the spirocycle could be readily converted into an indole enabling a direct scaffold hop of medicinal compounds. The model spirocycle **5e** was found to undergo conversion to the desired product in good yields when exposed to phenylhydrazine and acetic acid at high temperatures. Additionally, we assessed **5e** under standard Baeyer-Villiger oxidation conditions to afford chiral  $\delta$ -lactone **7**. Quinoline **8** also represents an important heterocyclic compound and we could access this motif via the Friedländer synthesis. Following these successful results, the last product diversification reaction focused on introducing new functional handles for potential further manipulation. Chloroformylation of **5e** by employing the Vilsmeier-Haack reagent led to structure **9** in good yields. As expected, ketone reduction with NaBH<sub>4</sub> and Grignard additions proceed with no levels of diastereocontrol (see SI). Overall, the transformations highlighted in Scheme 4 encompass a significant expansion in spirocyclic chemical space.

**Scheme 4.** Elaboration of the Prins-semipinacol spirocycle products.



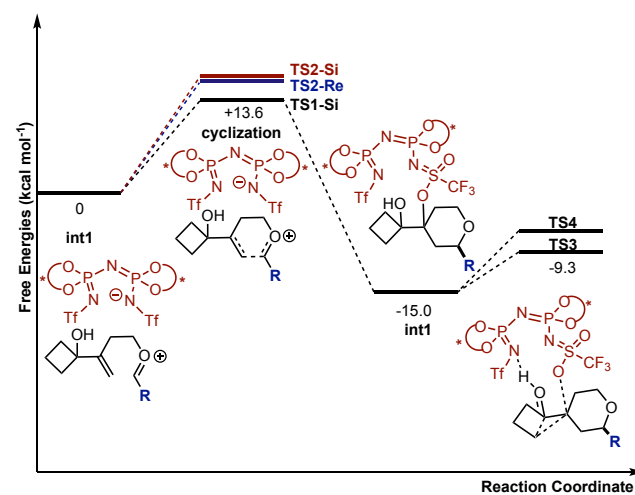
a) **5e** (0.1 mmol, 1.0 eq), PhNHNH<sub>2</sub>HCl (0.15 mmol, 1.5 eq), HOAc (0.25 mL), 120 °C, 4 h. (b) **5e** (0.1 mmol, 1.0 eq), m-CPBA (0.15 mmol, 1.5 eq), NaHCO<sub>3</sub> (0.3 mmol, 3.0 eq), DCM (2.0 mL), rt, 24 h. (c) **5e** (0.1 mmol, 1.0 eq), 2-aminobenzaldehyde (0.15 mmol, 1.5 eq), KOH (1 mmol, 10 eq), EtOH (1.0 mL), 80 °C, 4 h. (d) POCl<sub>3</sub> (0.1 mL), DMF (0.1 mL), 0 °C, 15 min; **5e** (0.1 mmol, 1.0 eq), DCM (2.0 mL), rt, 24 h. All reactions proceed with no erosion in selectivity. Isolated yields given. Enantioselectivities (ee) were measured by SFC.

**Mechanistic Studies.** The first part of the study accomplished two of our three initial goals; i.e., developed a selective catalyst, IDPi 2a, to facilitate a challenging reaction that had yet to be accomplished asymmetrically. Of note, this catalyst was thoughtfully designed by transferring well-performing substituents between unique eras of Brønsted acid catalyst structures and the feasibility for synthesis analyzed by considering its size relative to other groups. However, the final goal, to establish if the same set of enantiodetermining discriminants that are a well-recognized feature of 9-phenanthryl derived phosphoric acids, a earlier Brønsted acid

catalyst design, also extend to this catalyst structure, was not yet realized. As a result, we next evaluated the reaction mechanism with the aim of revealing the noncovalent interactions at the core of enantioinduction. In considering the complexity of the transformation, i.e., the cyclization or the rearrangement could be enantiodetermining and the large size of the structures that are required to be evaluated, we limited our analysis to the steps that follow the formation of the oxonium ion while also employing ONIOM( $\omega$ B97XD/6-31G(d,p):UFF) as the calculation method. This type of calculation allows larger systems like IDPi's to be explored efficiently without having the analysis limited to a few structures or a portion of the reactive systems.<sup>23</sup> While these computational methods have been shown to give reliable results in various settings including those involving IDPi's - we were aware of the possibility of error.<sup>24-28</sup> Accordingly, the lowest energy structures found in the enantiodetermining step using this method were submitted to full DFT geometry optimizations functionals to confirm the validity of our ONIOM results. The results of full DFT calculations can be found in the Supporting Information and show that interpretation of ONIOM structures and energies to be accurate.

Evaluation of the potential energy surface shows that the cyclization event proceeds with an energy barrier of 13.6 kcal/mol. This value is significantly higher than the computed barrier of 5.7 kcal/mol found for the rearrangement step. Low energy transition state (TS) structures

**A.** Calculating the energy barriers for cyclization and rearrangement



**B.** Measuring SKIE

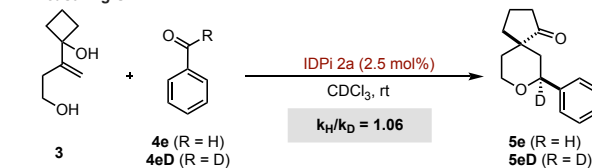


**Figure 3.** Determining the origin of enantioinduction (A) with ONIOM calculations and (B) with experimental rates.

located at the rearrangement step suggests that the reaction features a S<sub>N</sub>2'-like displacement of the catalyst structure. While these structures where the catalyst directly attacks

the electrophile have been observed in other systems it is typically associated with catalyst decomposition. Subsequent HRMS analysis (see SI for details) confirmed the presence of int2 providing strong evidence for this pathway. Another potentially valuable piece of information would be the measurement of a secondary kinetic isotope effect (SKIE). This task was accomplished using 4e and the corresponding 4eD as a probe. If the cyclization step was rate-determining, we should observe an inverse SKIE ( $K_h/K_D < 1$ , due to hybridization change of  $sp^2$  to  $sp^3$ ) or no effect. The KIE was measured to be 1.06 which could suggest that the formation of the oxonium ion is the rate determining step. This would also explain the rate dependencies observed with electron withdrawing substituents and explain the lack of reactivity with aliphatic substrates (see SI). Further, the barrier for cyclization using 4aD was evaluated computationally and this was found to, as expected, lead to an inverse SKIE (i.e. computed barrier to cyclization is slightly lower for 4aD than 4a). Overall, taken together the computations and mechanistic experiments support an enantiodetermining cyclization event. Further, the calculations corroborate both the observed high levels of enantio- and diastereoselectivity as well as the sense of induction (Figure 3).

To gain further insight into how the optimal IDPi imparts such high levels of enantioselectivity we further analyzed the key Prins reaction event (Table 2 and Figure 4). We calculated the lowest energy TS structure, TS1-Si, to bind to the catalyst through two hydrogen bonding interactions. The lower energy of a TS which establishes hydrogen bonding interactions with both the alcohol and the oxonium hydrogen is expected, as double coordination modes are most likely.<sup>29</sup> Comparable TS structures could be located in which the reactants establish only one of the hydrogen bonding contacts, TS2-Si, and these would also lead to the experimentally observed enantiomer but are higher in energy.

In addition, we identified TS structures similar to TS1-Si which features the interaction from the catalyst to the oxonium proton, TS1-Re, but affords the competing product. Further visual analysis reveals the most important difference between TS(Si) and TS(Re) is the absolute location and orientation of the 9-phenanthryl groups relative to the substrate. Visualization of TS(Si) shows that both structures position the substrate to maximize CH- $\pi$  interactions with the aromatic groups. In contrast, TS(Re) forces the substrate to occupy the empty space between the large 9-phenanthryl substituents. This is consistent with the primary determinants of enantioselectivity arising from these competing pathways being attractive noncovalent interactions with the 3,3' catalyst substituents and the substrate.<sup>30</sup> This is in agreement with the catalyst trends observed with earlier Brønsted acid designs bearing the same large, polarizable substituents. Excitingly, this suggests that the 9-phenanthryl groups do not have specific interactions when appended to a different Brønsted catalyst framework, even when placed in unique reaction settings.

The reasons for the energy differences between TS(Si) and TS(Re) were further investigated using distortion-interaction analysis (Table 2).<sup>31</sup> The equation  $\Delta\Delta E^\ddagger = \Delta\Delta E_{\text{int}} - \Delta\Delta E_{\text{distortCat}} - \Delta\Delta E_{\text{distortSub}}$  allows the relative energy difference between the three TS structures to be understood

partly on the basis of the energy required to distort the catalyst and substrate structures to the TS geometry, shown as the two  $\Delta\Delta E_{\text{distort}}$  terms. The interactions between the catalyst and substrate often represent a myriad of contacts with the total contribution appearing as  $\Delta\Delta E_{\text{int}}$  in the equation. The IEFPCM( $\text{CHCl}_3$ )- $\omega$ B97XD/6-311G(d,p) calculated difference in substrate distortion energy between TS(Si) and TS(Re) is small. However, the computed distortion energy difference for the catalyst fragment is significant. In fact, the catalyst structure must distort considerably more to achieve the low energy TS(Si) structures. The nature of this distortion is most easily visualized by overlaying the catalyst structures. Briefly, TS1-Si requires reorganization of the 9-phenanthryl groups to accommodate the substrate in the catalyst pocket. This is indicated in Figure 4B, where some of the catalyst groups of the green (TS2-Si) and blue (TS1-Si) structures take different positions. Overall, this clear difference in  $\Delta\Delta E_{\text{distortCat}}$  implies that the stabilization of TS1-Si relative to both TS2-Si and TS1-Re can be understood on the basis of favorable interaction energies, in agreement with our visual analysis of the competing TS structures. The  $\Delta\Delta E_{\text{int}}$  values demonstrate these constructive contacts between catalyst and substrate are greater in TS1-Si than TS2-Si which is unsurprising since TS2-Si lacks the second strong hydrogen bonding contact between the catalyst and the oxonium proton. Therefore, the high levels of enantioselectivity and overall sense of stereoreinduction can be explained by differences in attractive noncovalent interactions. Ultimately, demonstrating that the principles underlying effective asymmetric catalysis involving 9-phenanthryl derived Brønsted acid structures are fundamentally the same.

**Table 2.** Results from distortion-interaction analysis calculated with IEFPCM( $\text{CHCl}_3$ )- $\omega$ B97XD/6-311G(d,p) single point energy evaluations. All relative energies reported in kcal mol<sup>-1</sup>.

	$\Delta\Delta E^\ddagger$	$\Delta\Delta E_{\text{int}}$	$\Delta\Delta E_{\text{distortCat}}$	$\Delta\Delta E_{\text{distortSub}}$
TS1-Re	4.7	12.7	-8.0	0
TS2-Si	1.7	4.3	-2.5	-0.1
TS1-Si	0	0	0	0

## Conclusion.

We have achieved an enantioselective Prins-semipinacol reaction using a sterically bulky IDPi designed through the careful evaluation of catalyst properties and investigated the unique capacity of this catalyst architecture to impart high levels of stereocontrol. Computational studies demonstrate attractive noncovalent interactions from aromatic groups on the catalyst and substrate to determine the enantioselectivity, a distinctive feature of the 9-phenanthryl substituent in Brønsted acid catalysis. These findings suggest a probable general phenomenon, whereby various

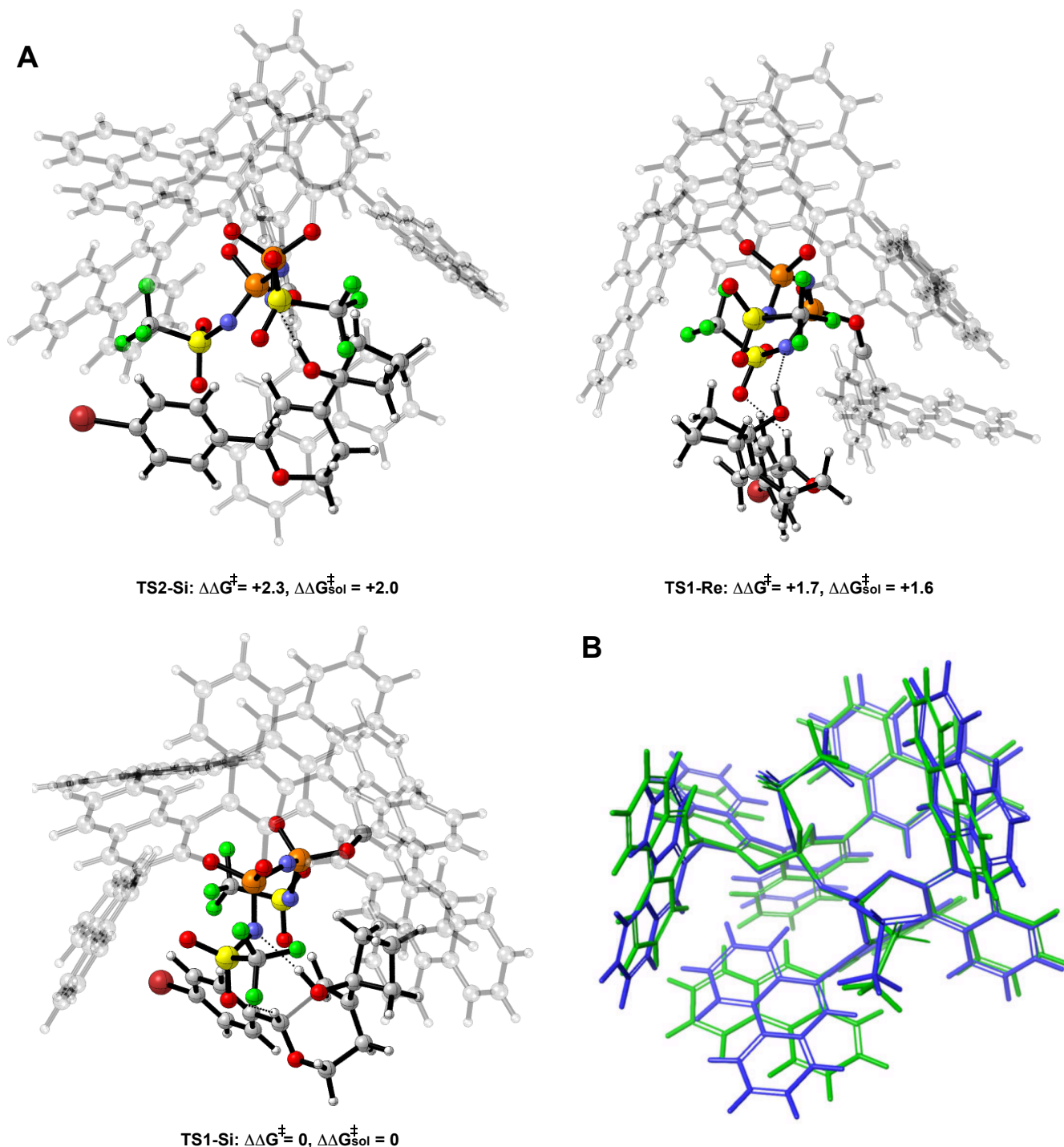


**Figure 4.** (A) Competing TS structures for the Prins reaction of homoallylic alcohol **3** with aldehyde **4a** and catalyzed by IDPi. ONIOM( $\omega$ B97XD/6-31G(d,p):UFF). Solvent energies were derived from single point energies with IEFPCM( $\text{CHCl}_3$ ) model at the  $\omega$ B97XD/6-311G(d,p) level. Grayed-out regions were treated with UFF, and the full-color regions were treated with  $\omega$ B97XD /6-31G(d,p). All energies quoted in  $\text{kcal mol}^{-1}$ . Key hydrogen bonding features shown in the gray box. (B) Superimposed, TS1-Si and TS2 -Si catalyst structures demonstrating the shifting of the 9-phenanthryl groups.



mechanistically unrelated transformations may be found to perform in the same manner when key catalyst groups are conserved between distinct eras of organocatalyst designs. Our ongoing and future studies are directed toward the generalization of substituent effects and leveraging this as a platform for catalyst design.

## ASSOCIATED CONTENT

### Supporting Information

Cartesian coordinates, energies of computed structures, experimental and X-ray crystal structure details (PDF).

## AUTHOR INFORMATION

### Corresponding Author

\* [jreid@chem.ubc.ca](mailto:jreid@chem.ubc.ca)

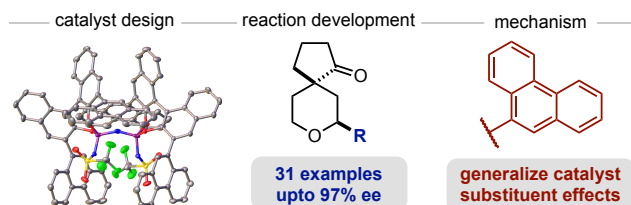
## ACKNOWLEDGMENT

Financial support to J.P.R. was provided by the University of British Columbia, the Natural Sciences and Engineering Research Council of Canada (NSERC) and the CFI John R. Evans

## REFERENCES

- (1) Doyle, A.G.; Jacobsen, E.N. Small-molecule H-bond donors in asymmetric catalysis. *Chem. Rev.* **2007**, *107*, 5713–5743. <https://doi.org/10.1021/cr068373r>
- (2) Han, B.; He, X.H.; Liu, Y.Q.; He, G.; Peng, C.; Li, J.L. Asymmetric organocatalysis: an enabling technology for medicinal chemistry. *Chem. Soc. Rev.* **2021**, *50*, 1522–1586. <https://doi.org/10.1039/D0CS00196A>
- (3) Kampen, D.; Reisinger, C. M.; List, B. Chiral Brønsted Acids for Asymmetric Organocatalysis. *Top. Curr. Chem.* **2010**, *291*, 395–456. [https://doi.org/10.1007/978-3-642-02815-1\\_1](https://doi.org/10.1007/978-3-642-02815-1_1)
- (4) Rueping, M.; Kuenkel, A.; Atodiressei, I. Chiral Brønsted acids in enantioselective carbonyl activations—activation modes and applications. *Chem. Soc. Rev.* **2011**, *40*, 4539–4549. <https://doi.org/10.1039/C1CS15087A>
- (5) Parmar, D.; Sugiono, E.; Raja, S.; Rueping, M. Complete field guide to asymmetric BINOL-phosphate derived Brønsted acid and metal catalysis: history and classification by mode of activation; Brønsted acidity, hydrogen bonding, ion pairing, and metal phosphates. *Chem. Rev.* **2014**, *114*, 9047–9153. <https://doi.org/10.1021/cr5001496>
- (6) Klussmann, M.; Ratjen, L.; Hoffmann, S.; Wakchaure, V.; Goddard, R.; List, B. Synthesis of TRIP and analysis of phosphate salt impurities. *Synlett* **2010**, *2010*, 2189–2192. <https://doi.org/10.1055/s-0030-1258505>
- (7) Čorić, I.; List, B. Asymmetric spiroacetalization catalysed by confined Brønsted acids. *Nature* **2012**, *483*, 315–319. <https://doi.org/10.1038/nature10932>
- (8) Mohammadlou, A.; Chakraborty, A.; Maday, M.; Yin, X.; Zheng, L.; Gholami, H.; Ashtekar, K.; Staples, R.; Wulff, W.; Borhan, B. Structure Guided Design of VANOL-imidodiphosphorimidate Catalysts for the Catalytic Enantioselective Bromo Spiroketalization Reaction. *ChemRxiv* **2023**. <https://doi.org/10.26434/chemrxiv-2023-2t3kl> June302023Accessed.
- (9) Nakashima, D.; Yamamoto, H. Design of chiral N-triflyl phosphoramidate as a strong chiral Brønsted acid and its application to asymmetric Diels–Alder reaction. *J. Am. Chem. Soc.* **2006**, *128*, 9626–9627. <https://doi.org/10.1021/ja062508t>
- (10) Schreyer, L.; Properzi, R.; List, B. IDPi catalysis. *Angew. Chem., Int. Ed.* **2019**, *58*, 12761–12777. <https://doi.org/10.1002/anie.201900932>
- (11) Schwengers, S.A.; De, C.K.; Grossmann, O.; Grimm, J.A.; Sadlowski, N.R.; Gerosa, G.G.; List, B. Unified approach to imidodiphosphate-type Brønsted acids with tunable confinement and acidity. *J. Am. Chem. Soc.* **2021**, *143*, 14835–14844. <https://doi.org/10.1021/jacs.1c07067>
- (12) Reid, J.P.; Goodman, J.M. Goldilocks catalysts: computational insights into the role of the 3, 3' substituents on the selectivity of BINOL-derived phosphoric acid catalysts. *J. Am. Chem. Soc.* **2016**, *138*, 7910–7917. <https://doi.org/10.1021/jacs.6b02825>
- (13) Reid, J.P.; Goodman, J.M. Selecting chiral BINOL - derived phosphoric acid catalysts: general model to identify steric features essential for enantioselectivity. *Chem.-Eur. J.* **2017**, *23*, 14248–14260. <https://doi.org/10.1002/chem.201702019>

## TOC GRAPHIC



- (14) Reid, J. P.; Ermanis, K.; Goodman, J.M. BINOPtimal: a web tool for optimal chiral phosphoric acid catalyst selection. *Chem. Commun.* **2019**, *55*, 1778-1781. <https://doi.org/10.1039/C8CC09344J>
- (15) Kaib, P.S.; Schreyer, L.; Lee, S.; Properzi, R.; List, B. Extremely active organocatalysts enable a highly enantioselective addition of allyltrimethylsilane to aldehydes. *Angew. Chem., Int. Ed.* **2016**, *55*, 13200-13203. <https://doi.org/10.1002/anie.201607828>
- (16) Gatzenmeier, T.; Turberg, M.; Yepes, D.; Xie, Y.; Neese, F.; Bistoni, G.; List, B. Scalable and highly diastereo- and enantioselective catalytic Diels–Alder reaction of  $\alpha$ ,  $\beta$ -unsaturated methyl esters. *J. Am. Chem. Soc.* **2018**, *140*, 12671-12676. <https://doi.org/10.1021/jacs.8b07092>
- (17) Lee, S.; Kaib, P.S.; List, B. Asymmetric catalysis via cyclic, aliphatic oxocarbenium ions. *J. Am. Chem. Soc.* **2017**, *139*, 2156-2159. <https://doi.org/10.1021/jacs.6b11993>
- (18) Bae, H.Y.; Höfler, D.; Kaib, P.S.; Kasaplar, P.; De, C.K.; Döhning, A.; Lee, S.; Kaupmees, K.; Leito, I.; List, B. Approaching sub-ppm-level asymmetric organocatalysis of a highly challenging and scalable carbon–carbon bond forming reaction. *Nature Chem.* **2018**, *10*, 888-894. <https://doi.org/10.1038/s41557-018-0065-0>
- (19) Maji, R.; Ghosh, S.; Grossmann, O.; Zhang, P.; Leutzsch, M.; Tsuji, N.; List, B. A Catalytic Asymmetric Hydrolactonization. *J. Am. Chem. Soc.* **2023**, *145*, 8788–8793. <https://doi.org/10.1021/jacs.3c01404>
- (20) Liu, L.; Kaib, P.S.; Tap, A.; List, B. A general catalytic asymmetric Prins cyclization. *J. Am. Chem. Soc.* **2016**, *138*, 10822-10825. <https://doi.org/10.1021/jacs.6b07240>
- (21) Díaz-Oviedo, C.D.; Maji, R.; List, B. The catalytic asymmetric intermolecular Prins reaction. *J. Am. Chem. Soc.* **2021**, *143*, 20598-20604. <https://doi.org/10.1021/jacs.1c10245>
- (22) Reddy, B.S.; Reddy, S.G.; Reddy, M.R.; Bhadra, M.P.; Sarma, A.V.S. Tandem Prins/pinacol reaction for the synthesis of oxaspiro [4.5] decan-1-one scaffolds. *Org. Biomol. Chem.* **2014**, *12*, 7257-7260. <https://doi.org/10.1039/C4OB01188K>
- (23) Chung, L.W.; Sameera, W.M.C.; Ramozzi, R.; Page, A.J.; Hatanaka, M.; Petrova, G.P.; Harris, T.V.; Li, X.; Ke, Z.; Liu, F.; Li, H.B. The ONIOM method and its applications. *Chem. Rev.* **2015**, *115*, 5678-5796. <https://doi.org/10.1021/cr5004419>
- (24) Reid, J. P.; Simón, L.; Goodman, J. M. A Practical Guide for Predicting the Stereochemistry of Bifunctional Phosphoric Acid Catalyzed Reactions of Imines. *Acc. Chem. Res.*, **2016**, *49*, 1029–1041. <https://doi.org/10.1021/acs.accounts.6b00052>
- (25) Reid, J. P.; Goodman, J. M. Transfer of *ortho*-hydroxybenzophenone ketimines catalysed by BINOL-derived phosphoric acid occurs by a 14-membered bifunctional transition structure. *Org. Biomol. Chem.* **2017**, *15*, 6943-6947. <https://doi.org/10.1039/C7OB01345K>
- (26) Simón, L.; Paton, R. S. The True Catalyst Revealed: The Intervention of Chiral Ca and Mg Phosphates in Brønsted Acid Promoted Asymmetric Mannich Reaction. *J. Am. Chem. Soc.*, **2018**, *140*, 5412-5420. <https://doi.org/10.1021/jacs.7b13678>
- (27) Simón, L.; Paton, R. S. QM/MM study on the enantioselectivity of spiroacetalization catalysed by an imidodiphosphoric acid catalyst: how confinement work. *Org. Biomol. Chem.* **2016**, *14*, 3031-3039. <https://doi.org/10.1039/C6OB00045B>
- (28) Lai, J.; Reid, J. P.; Interrogating the thionium hydrogen bond as a noncovalent stereocontrolling interaction in chiral phosphate catalysis. *Chem. Sci.* **2022**, *13*, 11065-11073. <https://doi.org/10.1039/D2SC02171D>
- (29) Caballero-García, G.; Goodman, J. M. N-Tri-*tert*-butylphosphoramides: highly acidic catalysts for asymmetric transformations. *Org. Biomol. Chem.*, **2021**, *19*, 9565-9618. <https://doi.org/10.1039/D1OB01708J>
- (30) Changotra, A.; Das, S.; Sunoj, R. B. Reversing Enantioselectivity Using Noncovalent Interactions in Asymmetric Dearomatization of  $\beta$  Naphthols: The Power of 3,3' Substituents in Chiral Phosphoric Acid Catalysts. *Org. Lett.* **2017**, *19*, 2354–2357. <https://doi.org/10.1021/acs.orglett.7b00890>
- (31) Bickelhaupt, F. M.; Houk, K. N. Analyzing Reaction Rates with the Distortion/Interaction-Activation Strain Model. *Angew. Chem., Int. Ed.* **2017**, *56*, 10070–10086. <https://doi.org/10.1002/anie.201701486>